Spinodal decomposition and dislocation lines in thin films and bulk materials

François Léonard and Rashmi C. Desai
Department of Physics, University of Toronto, Toronto, Ontario, Canada M5S 1A7
(Received 9 February 1998)

Phase separation of alloys around dislocation lines due to edge- and screw-type dislocations is studied using a continuum model. The dependence of the lattice constant, bulk modulus, and shear modulus on composition is shown to determine the distribution of the alloy components in the stress fields of the dislocations. Numerical simulation results are also presented for single dislocation lines, arrays of dislocations, and random distributions of dislocations in bulk mixtures in a context relevant to quench-work-age thermomechanical treatment of alloys. The effects of dislocations on the phase separation occurring at the surface of growing films is also discussed, showing that misfit dislocations can create a compositionally patterned layer. The equilibrium position of misfit dislocations is also calculated for compositionally modulated overlayers, and it is shown that the critical thickness for the introduction of dislocations is reduced due to the composition modulation. [S0163-1829(98)01037-6]

I. INTRODUCTION

It is well known that the strength of real solids is orders of magnitude less than the values predicted for perfect crystals. This is because the strength of a solid material is related to the density of dislocations, which can vary widely due to the preparation of the specimen. The simplest kinds of dislocations are known as edge- and screw-type dislocations, and their presence creates strong elastic deformations of the crystal in the vicinity of the dislocations and extending to large distances. Elastic deformations can also occur in alloys due to the dependence of the lattice constant or the elastic moduli on the local concentration of the alloy components. Hence, an interesting coupling arises between the elastic fields due to concentration inhomogeneities and the stress fields of the dislocations. This coupling between the composition of the alloy and the position of the dislocations was first considered[1] in the context of crystal hardening by the addition of solute atoms, the later being regarded as elastic inclusions in the matrix. The formation of clouds of solute particles *around* the dislocations was predicted, as well as their effect on dislocation motion. Later,[2] the nucleation of the precipitates *around* the dislocation lines was studied from a free-energy approach. A different perspective[3,4] on the nucleation problem showed an increased nucleation rate of precipitates *on* dislocations.

The studies described above focus on alloys quenched in the metastable region of the binary alloy phase diagram where the phase separation proceeds by nucleation and growth of precipitates. However, for an alloy quenched inside the spinodal region of the phase diagram, the phase segregation proceeds through spinodal decomposition. The interplay of spinodal decomposition and dislocations was explored by Cahn,[5] with interest on the effects of the decomposition on the dislocation motion and hardening. Experiments on moving dislocations in spinodal alloys have been presented in the literature.[6] The effects of thermomechanical treatment on the properties of decomposing alloys have shown the important coupling between dislocations and decomposition, and the possibility of enhanced kinetics of spinodal decomposition.[7–9] To our knowledge, the role played by immobile dislocations in the spinodal decomposition process and the spatial distribution of the decomposed products around the dislocation lines is still an open question.

Of practical importance is the role played by dislocations during the growth of thin films by deposition techniques.[10] There, a thin layer of material is deposited on a substrate of different lattice constant. The strain in the overlayer due to the lattice mismatch is eventually relieved by the introduction of misfit dislocations at a critical film thickness;[11,12] the film is then believed to contain arrays of edge dislocations at the film/substrate interface for which there is extensive experimental evidence. In the case of an *alloy* grown by molecular-beam epitaxy, both alloy components are simultaneously deposited on the substrate, which can lead to the decomposition of the alloy and the formation of ordered phases.[13] The effects of the dislocation array introduced at the critical thickness on this surface phase separation is studied in the present work.

In this paper, we first present a continuum theory that describes a binary alloy, phase separating by spinodal decomposition around edge- and screw-type dislocations. The dislocations are immobile; their role is to create a constant elastic deformation of the crystal that couples with the concentration fluctuations. We consider the cases of single dislocations, regular arrays of dislocations and random distributions of dislocations. A Ginzburg-Landau free energy is used to describe the thermodynamics of the alloy, while the deformation of the solid is considered within linear elasticity theory. Since the diffusion of material is much slower than lattice rearrangements, mechanical equilibrium is assumed to be satisfied at all times, allowing us to eliminate the displacement vector in favor of the concentration variable. In Sec. II, we present the model in more detail. In Sec. III, we discuss the results of numerical integration of our model. Section IV focuses on the growing film, presenting the derivation of the dynamical equations describing the time evolution of the surface phase separation as well as numerical integration of these equations. We include as well a discussion of the equilibrium position of misfit dislocations at the interface of a

substrate and a compositionally modulated overlayer, and we calculate the critical thickness for the introduction of misfit dislocations in these films. Section V describes our conclusions.

II. MODEL FOR BULK SYSTEMS

The extent of the phase separation is described by a local, continuous order parameter $\psi(\mathbf{r})$, proportional to the local difference in the concentration of the two species at position $\mathbf{r}$. Its energetics are given by the Ginzburg-Landau free-energy functional

$$\mathcal{F}_{GL}\{\psi\}=\int d\mathbf{r}\left[-\frac{r'}{2}\psi^2+\frac{u}{4}\psi^4+\frac{c}{2}|\nabla\psi|^2\right], \qquad (1)$$

with the coefficient r' proportional to T_c-T, T_c being the critical temperature of the binary alloy. The displacement vector $\mathbf{u}(\mathbf{r})$, represents the elastic deformations around the local equilibrium position, and $\mu_{ij}=(\nabla_i u_j+\nabla_j u_i)/2$ is the strain tensor. The elastic energy for an isotropic medium reads[14]

$$\mathcal{F}_{el}\{\psi,\mathbf{u}\}=\int d\mathbf{r}\left[\frac{1}{2}K(\nabla\cdot\mathbf{u})^2+M\sum_{i,j}\left(\mu_{ij}-\frac{\delta_{ij}}{3}\nabla\cdot\mathbf{u}\right)^2+\alpha\psi\nabla\cdot\mathbf{u}\right], \qquad (2)$$

with the last term added to describe the dependence of the lattice constant on composition. The lattice constant depends on ψ through the relation $\ln a=-\alpha\psi/3K$, implying that for $\alpha>0$ the lattice constant is smaller for $\psi>0$. The dependence of the lattice constant on composition is often written in terms of the solute expansion coefficient η as $a=\overline{a}(1+\eta\psi)$, leading to $a^{-1}\partial a/\partial\psi=\eta=-\alpha/3K$. The bulk modulus K and the shear modulus M depend on composition as $K=K_0+K_1\psi$ and $M=M_0+M_1\psi$, with K_1 and M_1 assumed to be small quantities.

A dislocation is described by a vector $\mathbf{n}$, parallel to the dislocation line, and by the Burgers vector $\mathbf{b}$ that satisfies

$$\oint d\mathbf{u}=-\mathbf{b}. \qquad (3)$$

The contour of integration in Eq. (3) encloses the dislocation line and is traversed in a direction consistent with the right-hand rule for the vector $\mathbf{n}$.

Since the local repositioning of atoms is much faster than their diffusion, we assume that mechanical equilibrium is satisfied at all times, such that the displacement vector instantaneously adjusts to a given spatial distribution of ψ. The differential equations for mechanical equilibrium in the presence of a dislocation and with compositional stresses are

$$M\nabla^2\mathbf{u}+(K+M/3)\nabla\nabla\cdot\mathbf{u}+\alpha\nabla\psi=M\mathbf{n}\times\mathbf{b}\,\delta(\boldsymbol{\xi}), \qquad (4)$$

where the vector $\boldsymbol{\xi}$ is a two-dimensional vector perpendicular to $\mathbf{n}$ with origin at the dislocation line. Solution of these equations gives $\mathbf{u}$ as a function of ψ, which can be used to rewrite the elastic free energy, Eq. (2), as a function of ψ only.

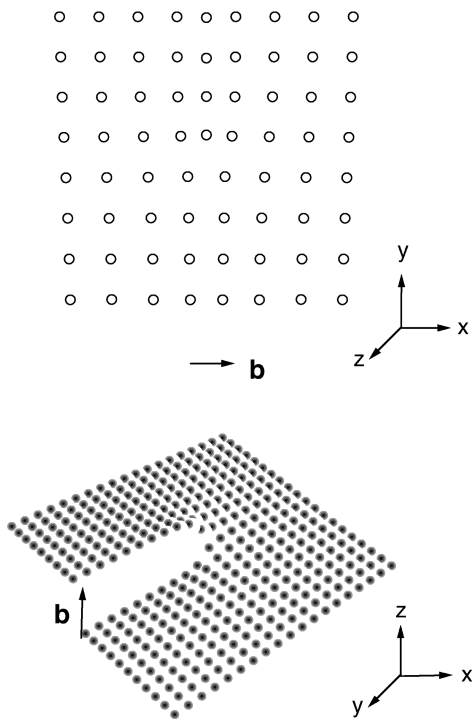

FIG. 1. The top figure shows representative points of a solid containing an edge dislocation. The dislocation can be viewed as the addition of an extra half plane of atoms in the upper half of the figure, corresponding to a Burgers' vector in the positive x direction. The bottom figure shows the displacements of representative points around a screw dislocation with Burgers' vector in the positive z direction. If one starts at a particular point and rotates counterclockwise by 360°, the final point will be one Bergers' vector above the starting point.

We now derive the effective free energy for edge and screw dislocations, doing so separately for the contributions from α, K_1, and M_1.

A. Edge dislocation

We consider an edge dislocation in the upper half of the xy plane corresponding to the addition of an extra half plane of atoms whose edge (the dislocation line) lies on the z axis (see Fig. 1). The vector $\mathbf{n}$ is constant along the dislocation line and is equal to $-\hat{\mathbf{z}}$ while the Burgers vector is in the x direction, $\mathbf{b}=b\hat{\mathbf{x}}$. The mechanical equilibrium equations are then

$$M\nabla^2\mathbf{u}+(K+M/3)\nabla\nabla\cdot\mathbf{u}+\alpha\nabla\psi=-Mb\hat{\mathbf{y}}\delta(x)\delta(y). \qquad (5)$$

The vector $\mathbf{u}$ can be separated in two parts, $\mathbf{u}=\mathbf{u}^d+\mathbf{u}^\psi$, where $\mathbf{u}^d$ is the solution in the absence of compositional stresses and $\mathbf{u}^\psi$ is the solution in the absence of the dislocation. The vector $\mathbf{u}^\psi$ and the effective free energy in the absence of $\mathbf{u}^d$ have been calculated in prior work.[13] Because of symmetry, $\mathbf{u}^d=(u_x^d,u_y^d,0)$ with u_x^d and u_y^d independent of z, and the strains and stresses due to the dislocation are entirely in the plane perpendicular to the dislocation line. We therefore consider the order parameter ψ to also be a two-dimensional field in the xy plane.

1. Composition-dependent lattice constant

In this case, $\alpha \neq 0$ and $K_1 = M_1 = 0$, implying that the alloy is elastically sensitive to local variations in the lattice constant only. Solution of Eq. (5) gives the displacement vector as

$$u_x = \frac{b}{2\pi}\left[\arctan\left(\frac{y}{x}\right) + D_0 \frac{xy}{x^2+y^2}\right] - \frac{\alpha}{C_0}\nabla_x \nabla^{-2}\psi, \quad (6)$$

$$u_y = -\frac{b}{2\pi}\left(\frac{M_0}{C_0}\log\sqrt{x^2+y^2} + D_0 \frac{x^2}{x^2+y^2}\right) - \frac{\alpha}{C_0}\nabla_y \nabla^{-2}\psi, \quad (7)$$

where $C_0 = K_0 + 4M_0/3$, $D_0 = (K_0 + M_0/3)/(K_0 + 4M_0/3)$ and ∇^{-2} denotes the inverse Laplacian. The first terms in these equations correspond to the usual lattice distortions due to the dislocation, while the second terms are due to the compositional variations. From these expressions for the displacements, we can calculate the compression and the shear strains in the solid:

$$\nabla \cdot \mathbf{u} = -\frac{b}{2\pi}\frac{2M_0}{C_0}\left(\frac{y}{x^2+y^2}\right) - \frac{\alpha}{C_0}\psi \quad (8)$$

and

$$\mu_{xy} = \frac{b}{2\pi} D_0 \frac{x(x^2-y^2)}{(x^2+y^2)^2} - \frac{\alpha}{C_0}\nabla_x \nabla_y \psi. \quad (9)$$

The compression and the shear strain contain contributions from the dislocation and from the composition inhomogeneities. The effective elastic free energy density can be written as a sum of three terms, $f = f_\psi + f_d + f_I$, where f_ψ is a function of ψ only, f_d is the energy of the dislocation and is independent of ψ, and f_I is the interaction energy between the composition field and the stress field of the dislocation. We find that

$$f_\psi = -\frac{\alpha^2}{2C_0}\psi^2 \quad (10)$$

and

$$f_I = -\alpha \frac{b}{2\pi}\frac{2M_0}{C_0}\psi \frac{y}{x^2+y^2}. \quad (11)$$

With these expressions, the total free-energy functional becomes (to within a constant coming from f_d)

$$\mathcal{F}\{\psi\} = \int d\mathbf{r}\left[-\frac{r}{2}\psi^2 + \frac{u}{4}\psi^4 + \frac{c}{2}|\nabla\psi|^2 - \beta'_\alpha \psi \frac{y}{x^2+y^2}\right], \quad (12)$$

with $r = r' + \alpha^2/C_0$ and $\beta'_\alpha = \alpha(b/2\pi)(2M_0/C_0)$. Hence, f_ψ simply renormalizes the coefficient of ψ^2. The interesting effect comes from f_I: it introduces a coupling between the local composition fluctuation ψ and its spatial position, which varies as $1/R$. For example, if $\alpha > 0$, then $\beta' > 0$ and the energy is minimized for ψ positive in the region $y > 0$. This is because the alloy is compressed in this region [see Eq. (8)] that is preferred by smaller atoms ($\psi > 0$). The R^{-1} dependence of the interaction energy between the order parameter and the dislocation line is in agreement with previous work in the context of elastic inclusions in a matrix.[15]

We now make the transformations $\mathbf{x} = (r/c)^{1/2}\mathbf{r}$, $\phi = (u/r)^{1/2}\psi$ and $\beta_\alpha = (u/cr^2)^{1/2}\beta'_\alpha$ to obtain the dimensionless free energy

$$\mathcal{F}\{\psi\} = \int d\mathbf{x}\left[-\frac{\phi^2}{2} + \frac{\phi^4}{4} + \frac{|\nabla\phi|^2}{2} - \beta_\alpha \phi \frac{y}{x^2+y^2}\right], \quad (13)$$

with the understanding that x and y are the rescaled spatial coordinates.

For an array of parallel edge dislocations with spacing d lying in the same slip plane, the rescaled interaction energy density generalizes to

$$f_I = -\beta_\alpha \phi \sum_{n=-\infty}^{\infty} \frac{y}{(x-nd)^2+y^2}. \quad (14)$$

A rough estimate of the magnitude of the contributions due to the edge dislocations can be obtained as follows. Using the regular solution model, the values of r, u and c can be expressed in terms of the critical temperature T_c and the number density N_v,[16] which allows us to express the rescaled interaction parameter as $\beta_\alpha \approx [k_B(T_c - T)N_v]^{-1}(T/T_c)^{1/2}(K_0/5)(\Delta a/a)(M_0/C_0)$. Order of magnitude values for the elastic constants are 10^{11} Nm^{-2} while the ratio $\Delta a/a$ is of the order of 0.02. Typical aging of the alloy well within the miscibility gap would correspond to values of $T = T_c/2$, which yields β_α of order 1 for T_c around 500 K.

2. Composition dependent bulk modulus

For a composition dependent bulk modulus only, $K_1 \neq 0$, $M_1 = 0$, $\alpha = 0$, the displacement vector and the free energy are calculated to first order in K_1.[13] The new interaction term in the energy is

$$f_I = \frac{1}{2}K_1 \psi (\nabla \cdot \mathbf{u}^0)^2 = 2\left(\frac{b}{2\pi}\right)^2 \frac{K_1 M_0^2}{C_0^2}\psi\left(\frac{y}{x^2+y^2}\right)^2, \quad (15)$$

where $\mathbf{u}^0$ is the zeroth-order displacement obtained by setting $\alpha = 0$ in Eqs. (6) and (7). Hence the rescaled interaction energy is $f_I = \beta_K \phi [y/(x^2+y^2)]^2$ with the dimensionless parameter $\beta_K = 2(b/2\pi)^2(K_1 M_0^2/C_0^2)(u/rc^2)^{1/2}$. Compared to the contribution from β_α in the previous section, the spatial field around the dislocation has a shorter range, varying as $1/R^2$. Also, since the bulk modulus is sensitive to the absolute value of the compression, the regions of maximum absolute value of the compression will be favored by $\phi < 0$.

3. Composition-dependent shear modulus

In the case $M_1 \neq 0$, $K_1 = 0$, and $\alpha = 0$, the corrections to the energy come from the shear part of the elastic energy:

$$f_I = 2M_1 D_0^2 \left(\frac{b}{2\pi}\right)^2 \psi \frac{\frac{1}{3}(M_0/C_0 D_0)^2 y^2 + x^2}{(x^2+y^2)^2}. \quad (16)$$

Again, the interaction decreases as $1/R^2$ around the dislocation line, with the regions where shear energy is a maximum preferred by $\psi<0$ if $M_1>0$. In dimensionless form, $f_I=\beta_M\phi[\frac{1}{3}(M_0/C_0D_0)^2y^2+x^2]/(x^2+y^2)^2$ with $\beta_M=2M_1D_0^2(b/2\pi)^2(u/rc^2)^{1/2}$.

B. Screw dislocation

The screw dislocation is oriented in the z direction with vectors $\mathbf{n}=-\hat{\mathbf{z}}$ and $\mathbf{b}=b\hat{\mathbf{z}}$, as shown in Fig. 1. The displacement $\mathbf{u}$ has only one component u_z that depends on the coordinates x and y only. This means that the stress and strain fields are pure shears, implying that the alloy constituents will be sensitive to the elastic fields of the dislocation only if the shear modulus is composition dependent. For the screw dislocation, the mechanical equilibrium equations reduce to

$$\nabla^2 u_z=0, \tag{17}$$

with solution

$$u_z=\frac{b}{2\pi}\arctan\left(\frac{y}{x}\right). \tag{18}$$

The interaction free-energy density is

$$f_I=\frac{M_1}{2}\left(\frac{b}{2\pi}\right)^2\psi\frac{1}{x^2+y^2}, \tag{19}$$

which decreases as $1/R^2$ and favors $M_1\psi<0$ near the dislocation. In a rescaled form, $f_I=\beta_S\phi/(x^2+y^2)$ with $\beta_S=(M_1/2)(b/2\pi)^2(u/rc^2)^{1/2}$. The results for screw *and* edge dislocations show that when the elastic constants of the alloy elements are different, the interaction energy between the order parameter and the dislocation line varies as R^{-2}, in agreement with previous calculations.[15]

III. NUMERICAL RESULTS

Suppose we initially prepare the system at a temperature above the critical point where the alloy components are homogeneously distributed in the solid. As the system is quenched below the critical point, spinodal decomposition is triggered by a long-wavelength instability of the homogeneous state. The dynamics of the spinodal decomposition are described by an equation for the time variation of the order parameter that conserves the volume fraction of the two species:

$$\frac{\partial\phi}{\partial t}=-\nabla\cdot\mathbf{J}_\phi=\nabla^2\mu_\phi=\Lambda\nabla^2\frac{\delta\mathcal{F}}{\delta\phi}, \tag{20}$$

where in this equation, $\mathbf{J}_\phi$ is a current, μ_ϕ is the chemical potential and Λ is a kinetic coefficient. With the time rescaling $\tau=(\Lambda r^2/c)t$, the full dynamical equation is

$$\frac{\partial\phi}{\partial\tau}=\nabla^2\left[-\phi+\phi^3-\nabla^2\phi+\frac{\partial f_I}{\partial\phi}\right]. \tag{21}$$

The numerical simulations were carried out by discretizing the above equation using an Euler scheme with mesh size $\Delta x=\Delta y=1.25$ and time step $\Delta\tau=0.1$. The systems were of size $128\Delta x\times128\Delta x$ with periodic boundary conditions and the initial state consisted of a random distribution of ϕ in the interval $[-0.1,0.1]$. The size of the system is large enough that, for single dislocation systems, the immediate neighborhood of the dislocation is not affected by the periodic boundary conditions. The single dislocations were located in the center of the system, while the array of dislocations was located on the line $y=0$.

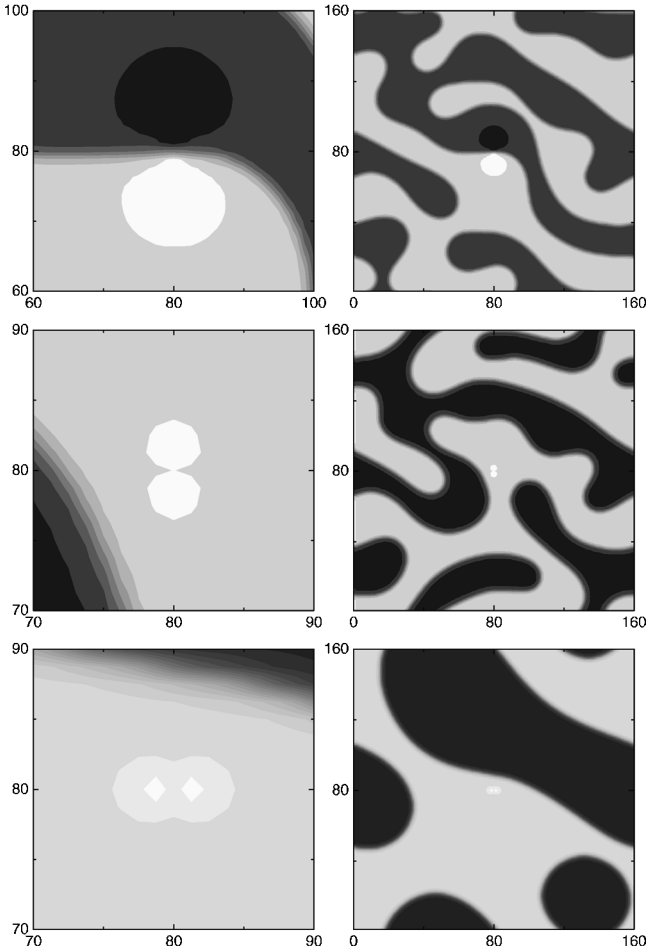

FIG. 2. Grey scale plot of the order parameter near the dislocation (left panels) and for the whole system (right panels). The dislocation is of edge type with dislocation line into the plane and in the center of the figures. The top row corresponds to the case where the lattice constant of the alloy depends on ϕ and provides the coupling with the stress field of the dislocation. The middle row is for the case when the bulk modulus is composition dependent, and the bottom row is for a composition-dependent shear modulus. In these and other figures, black is the largest positive value of ϕ and white the most negative value. The spacing between the gray shades corresponds to a change in the order parameter values of 0.35. Time is $\tau=3000$.

A. Single edge dislocation

The top row in Fig. 2 shows the order parameter for the full system and for the region around the dislocation in the case when the coupling between the concentration and the dislocation stress field arises due to the dependence of the lattice constant on ϕ. The coupling constant $\beta_\alpha=2$ in this simulation. Since the dislocation creates a compression of the lattice constant for $y>0$ and a dilatation for $y<0$, the

smaller atoms accumulate preferentially above the dislocation line while larger atoms accumulate below the dislocation line. Because $\beta_\alpha > 0$, the smaller atoms are represented by positive values of ϕ (black in the figure) and the larger atoms correspond to negative values of ϕ (white in the figure). For A- and B-type atoms in a binary alloy, a three-dimensional view of the system would show tubes of A- and B-type atoms above and below the dislocation line, parallel to the dislocation. These tubes are analogous to the solute atmospheres predicted by Cottrell.[1] We note that the extent of the distribution around the dislocation (about 15 dimensionless units) is much larger than the thickness of interfaces between order parameter domains for the value of β_α used in our simulations. Since β_α depends on the temperature as $(T_c - T)^{-1}$, the proximity to the critical point determines whether the anisotropic segregation will be observable experimentally.

The middle panels in Fig. 2 are gray scale plots of the order parameter when the bulk modulus is composition dependent ($\beta_K = 2$). The regions where $|\nabla \cdot \mathbf{u}|$ is maximum, just above and below the dislocation line, are favored by the component with the smallest bulk modulus, in this case $\phi < 0$. As compared to the top panels in Fig. 2, the size of the segregation region around the dislocation line is smaller since the interaction energy decays as $1/R^2$ instead of $1/R$. Also, there is no order parameter interface near the dislocation as in the top panels of Fig. 2; the immediate neighborhood of the dislocation is composed primarily of one component.

The bottom panels in Fig. 2 show the distribution of the alloy constituents when the composition-dependent shear modulus provides the coupling with the dislocation. The parameter $\beta_M = 2$ and the ratio $M_0/(C_0 D_0) = 1/2$, corresponding to a Poisson ratio of 1/4. With this choice for the parameters, the term proportional to y^2 in the numerator of Eq. (16) is much smaller than the term x^2, and this creates the preferred segregation in the x direction in Fig. 2.

In general, the lattice constant, the bulk modulus and the shear modulus all depend on the order parameter, and the three effects discussed above are present. However, the ratios β_K/β_α and β_M/β_α are roughly of order K_1/K_0 and M_1/M_0 respectively, which are assumed to be small quantities in this work, implying that the effects due to the dependence of the lattice constant on composition should be dominant.

B. Single screw dislocation

In the case of a pure screw dislocation, the interaction energy is given by Eq. (19). Simulation results are presented in the top row of Fig. 3 for $\beta_S = 2$, showing the isotropic segregation of one of the components around the dislocation. Because the lattice deformation due to the dislocation is a pure shear and is more pronounced near the dislocation line, the component of the binary alloy with the lowest shear modulus ($\phi < 0$ in the simulations) is attracted to the vicinity of the dislocation line. Here, because the deformation is a pure shear, the effect of the composition-dependent shear modulus is the only observable effect, with the parameter β_S roughly of order $M_1/r^{1/2}$. Since r is proportional to $T_c - T$, β_S can be made arbitrarily large by approaching T_c. A three-dimensional view would show a tube of one component wrapping the dislocation line.

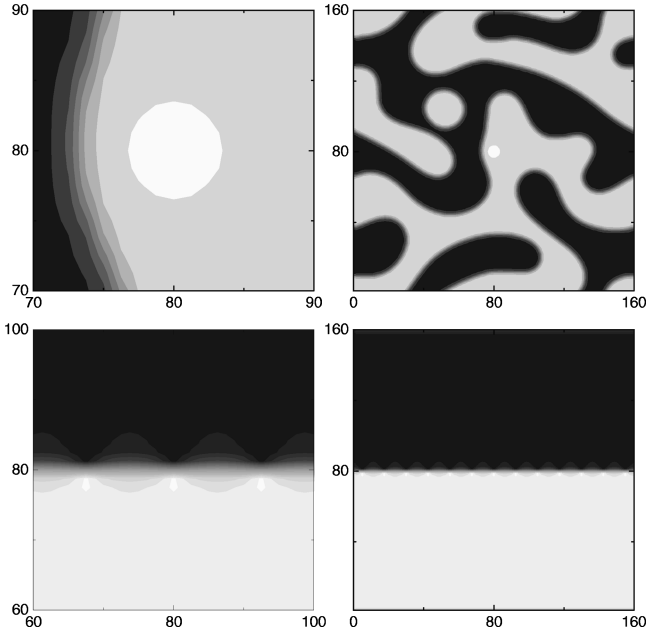

FIG. 3. Top row: grey scale plot of the order parameter phase separating around a screw dislocation with dislocation line coming out of the plane of the figure. As discussed in the text, the difference in the shear moduli of the two alloy components is responsible for the preferential segregation of one of the components near the dislocation line. Bottom row: complete phase separation of the alloy components when an infinite array of edge dislocations lies on the x axis. The spacing between the dislocations is $10\Delta x$, and the time is $\tau = 3000$. The spacing between the gray shades corresponds to a change in the order parameter values of 0.35.

C. Array of edge dislocations

The effects of an array of parallel edge dislocations on the phase separation are shown in the lower panels of Fig. 3. In this figure, the Burgers vectors of the dislocations are of equal magnitude and oriented in the positive x (horizontal) direction. The spacing d between the center of the dislocation lines is $10\Delta x$. Again, the smaller atoms are attracted to the region above the dislocation line because of the elastic compression there. The presence of the dislocation line provides a location of choice for the interface between the separating components, leading to a rapid separation of the two components (compare with Fig. 2 plotted at the same time). In fact, the density of dislocation lines along the array is an important parameter determining the rapidity of the spinodal decomposition, as shown in Fig. 4, where we plot the first moment of the structure factor $k(\tau) = \int k S(k,\tau) dk / \int S(k,\tau) dk$. The structure factor is defined as $S(k,\tau) = \langle \phi(k,\tau) \phi(-k,\tau) \rangle$. The dominant length scale in the system, $R(\tau) \sim 1/k(\tau)$, represents the size of the phase separating domains. As can be seen in the figure, the closer the spacing between dislocations (higher density) the faster the decomposition of the alloy.

D. Random distribution of dislocations

It is clear from the discussion above that the presence of a dislocation affects the phase separation in the vicinity of the

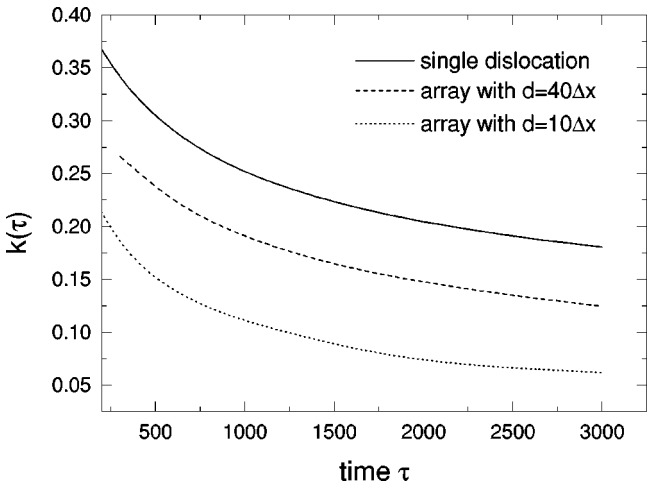

FIG. 4. Wave number as a function of time for an array of edge dislocations along the x axis. The decomposition is accelerated as the density of dislocations increases.

dislocation. In the case of the array of edge dislocations, the array provides a preferred location for the interface between the two coexisting phases. Because the dislocation lines were equally spaced and their Burgers' vectors were the same (sign and magnitude), there is a cooperative effect of the dislocations on the spinodal decomposition. We now turn to the case of a random spatial distribution of parallel dislocation lines with a random orientation of their Burgers' vector in the $\hat{\mathbf{x}}$ or $-\hat{\mathbf{x}}$ direction for edge dislocations. The systems are two dimensional as before, and the density of dislocations is measured as the number of dislocations per Δx^2. Figure 5 shows a black and white plot of the order parameter for a system with edge dislocations evolving from $\tau=100$ to $\tau=3000$. The dislocations are represented by gray dots and have two possible orientations for the Burgers' vector. The panels on the left represent an alloy with a density of dislocations of 0.01, while the pictures on the right are for a dislocation-free solid. It is obvious from these pictures that the overall morphology of the phase separation pattern is affected by the uncooperative stress fields of the dislocations. Because a positive (negative) edge dislocation produces a stress field that favors larger atoms above (below) it, the dislocations tend to be located at the interface between phase separating domains at early times. Since we have chosen the Burgers' vector of the dislocations to be oriented in the $\pm\hat{\mathbf{x}}$ direction, the formation of interfaces primarily on dislocations creates an anisotropy in the x direction that creates elongated domains. As time proceeds, the phase separation is strong enough to drive the interfaces through the dislocation network thereby increasing the domain size as a function of time. Even when this happens, the interface can remain pinned to a dislocation, and the interface between domains is rough as compared to the dislocation-free case. We have monitored the time evolution of the first moment $k(\tau)$ of the structure factor as a function of the density of dislocations, as shown in Fig. 6. It can be seen that the phase separation is in fact faster when the density of dislocations increases. The shape of the $k(\tau)$ curves shows however that the acceleration of the phase separation occurs at early times and that the subsequent time evolution proceeds very similarly to the phase separation without dislocations. This is further demonstrated in the inset to Fig. 6, where we plot the wavenumber as a function of dislocation density for two times, $\tau=500$ and $\tau=3000$ for the random distribution of dislocations *and* for the linear array of equally spaced dislocations studied in the previous section. This plot shows that the dependence of k on the density is the same for these two times.

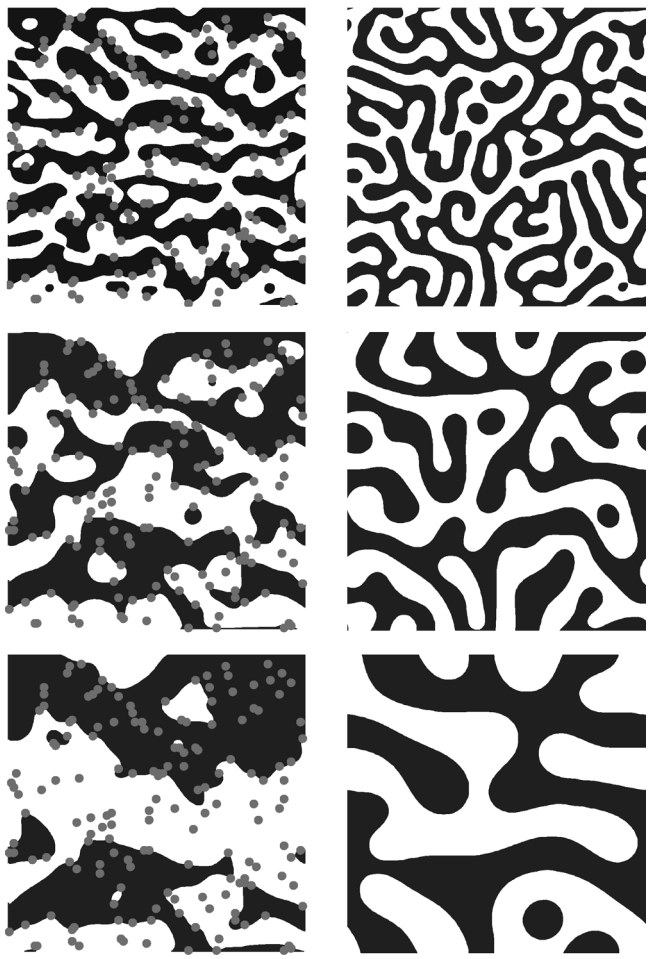

FIG. 5. Phase separating alloys at different times of their dynamical evolution. Panels from top to bottom correspond to the times $\tau=100$, 500, and 3000. The alloy on the left has an areal density of dislocations of 0.01 (area measured in units of Δx^2) while the alloy on the right is dislocation-free. The dislocations are represented by grey dots and the regions where $\phi>0$ ($\phi<0$) are white (black). Both alloys were started with the same initial conditions.

The acceleration of spinodal decomposition in the presence of dislocations has been discussed in the experimental literature as stated in the Introduction. In recent studies of the thermomechanical treatment of CuNiCr alloys,[7] it was reported that spinodal decomposition was accelerated in samples that were deformed prior to aging as compared to undeformed samples. The deformation before aging introduces a large number of dislocations in the sample indicating the direct correspondence between the density of dislocations and the enhanced decomposition, in agreement with the results of the present study. It was postulated that the faster spinodal decomposition is due to an increase in the diffusional flux due to the large density of dislocations; our work clearly shows that the diffusion potential is modified by the presence of dislocations and that the contributions to the lo-

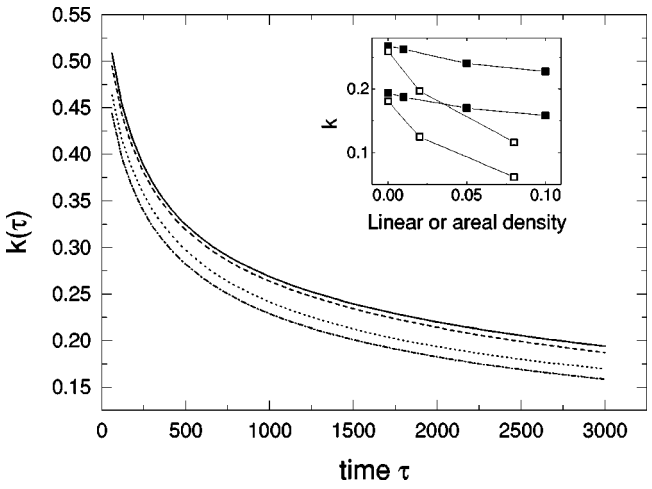

FIG. 6. Time evolution of the wave number for various values of the density of dislocations (measured per Δx^2). The curves from top to bottom are for dislocation densities of 0, 0.01, 0.05, and 0.1. The inset shows k at times $\tau=500$ (top curves) and at $\tau=3000$ (bottom curves) for the systems with a random distribution of dislocations (solid squares) and for the system with an array of dislocations (open squares).

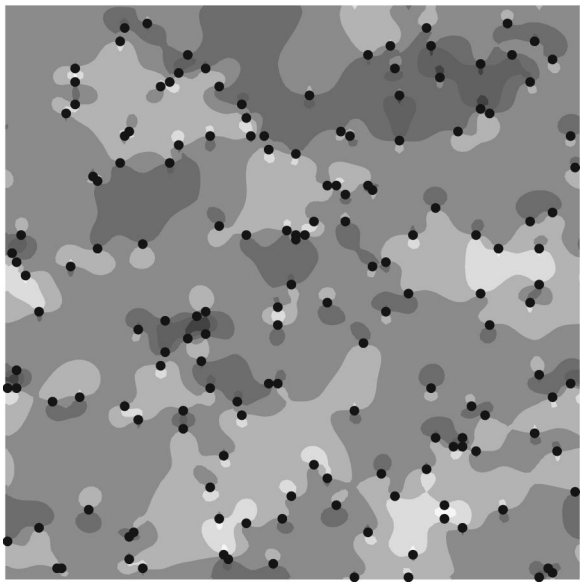

FIG. 7. Equilibrium distribution of the order parameter when the alloy is outside of the two-phase region of the coherent alloy. The black dots represent edge dislocations. In the absence of dislocations, the system would be homogeneous and the figure would be entirely of the same gray shade. The maximum absolute value of the order parameter is 0.1.

cal chemical potential due to the dislocations produce a rapid segregation of the alloy components. Furthermore, the time dependence of k was also studied[7] and agrees with our findings that at a given time k is smaller when the dislocation density is higher and that the differences in the time evolution of k occur at the early times of the aging process. Also, the rate of coarsening was found not to be affected by the dislocations at later times, in agreement with our numerical simulations. An alternate explanation for the acceleration of spinodal decomposition in cold-worked alloys is as follows: cold work can increase the concentration of vacancies above the equilibrium concentration, and hence, increase the diffusion coefficient. This increase in the diffusion coefficient would accelerate the decomposition of the alloy. Experiments can be performed to distinguish between these two scenarios by measuring the rate of coarsening as a function of the dislocation density.

We conclude this section by noting that the preferred segregation of the two components in the stress field of the dislocations also occurs for alloys outside of the two-phase region of the phase diagram. This is illustrated in Fig. 7, which shows the equilibrium profile of the alloy components in a random distribution of edge dislocations. In the absence of the dislocations, the alloy would be perfectly homogeneous and Fig. 7 would be entirely gray. Because the dislocations introduce a stress field, a *weak* inhomogeneity appears in the order parameter distribution. The weakness in this segregation is due to the fact that the elastic energy relieved is in competition with the entropic contributions that tend to homogenize the system.

IV. GROWING THIN FILM

In this section we discuss the application of the results of the previous section to thin films. We first briefly discuss the equilibrium position of misfit dislocations at the interface between a substrate and a thin film that is compositionally modulated. We then turn our attention to a growth process where the appearance of arrays of misfit dislocations can be used to compositionally pattern a growing film.

One of the possible mechanism to relieve the strain in mismatched systems is the bending of dislocation lines into the substrate/film interface. If the overlayer is modulated with $\psi=A\cos[q(x-x_0)]$, then the question we ask is what is the equilibrium position of the dislocation when it is bent into the interface? This can happen, for example, when a binary alloy is deposited directly onto a mismatched substrate, since the phase separation will occur at the onset of the deposition and the introduction of the misfit dislocations will occur later (at the critical thickness for example). Neglecting the fact that the actual solution of the mechanical equilibrium equations would require that the growing surface be free, the energy to be minimized is the interaction energy between the order parameter and the stress field of the dislocation, the f_I of the previous sections. For a film under *tensile* strain growing in the y direction, and with an edge dislocation with Burgers' vector in the x direction and located at $(x,y)=(0,0)$ the total energy per unit length is given by [see Eqs. (11) and (12)]

$$F=-\beta'_\alpha A\int_{-\infty}^{\infty}\int_0^h \cos[q(x-x_0)]\frac{y}{x^2+y^2}dydx, \quad (22)$$

where we have considered only the lattice constant to depend on ϕ. Evaluation of the integral leads to

$$F=-\beta'_\alpha A\left(\frac{1-e^{-qh}}{q}\right)\cos(qx_0), \quad (23)$$

implying that, for β'_α, the minimum is when $\cos(qx_0)=1$, or $x_0=0,2\pi/q,\ldots$, independently of the value of the modulation wavelength or of the film thickness (since the prefactor

in F never changes sign as q or h is varied). If the overlayer is viewed as being made of alternating stripes of the alloy constituents, then the equilibrium position of the dislocation line is at the center of a stripe with the smallest lattice constant (note that because the energy is always negative, a dislocation line perpendicular to the modulation will always have a smaller energy than a dislocation line parallel to the composition modulation). There exists the possibility that dislocations that do not bend into the interface to relieve the misfit strain extend to the surface and have a dislocation line that is perpendicular to the surface. In such a case, the free energy per unit length of the dislocation (edge type with Burgers' vector $\mathbf{b}=\hat{\mathbf{x}}$ and located at the origin) in the presence of a composition modulation in the z direction is

$$F=-\frac{2\pi\beta'_\alpha A}{q}\sin(qz_0), \tag{24}$$

implying that the equilibrium location of the dislocation is at the interface between the compositional domains.

We can estimate, using energy minimization arguments,[11] the critical thickness of the compositionally modulated growing film when the introduction of the misfit dislocations will occur. Our goal is to show that the composition modulation can decrease the critical thickness by considering the introduction of the first misfit dislocation. The energy per unit length of one misfit dislocation located at its equilibrium position is

$$\mathcal{E}=\frac{Mb^2}{4\pi(1-\nu)}\ln\left(\frac{4h}{b}\right)-2M|\varepsilon|b\left(\frac{1+\nu}{1-\nu}\right)t -|\beta'_\alpha|A\left(\frac{1-e^{-qh}}{q}\right), \tag{25}$$

where ε is the misfit between the film and the substrate, and ν is the Poisson ratio. The first two terms are the energy contributions for a dislocation in a homogeneous film,[11] while the last term in this equation accounts for the composition modulation and is the new effect of interest here. Because this term is always negative, the energy of the dislocation is reduced by its presence, implying that the introduction of the dislocation will occur earlier. We now make the rescaling $h^*=h/b$, $k=qb$ and define the parameters

$$S=[8\pi(1+\nu)]^{-1} \quad \text{and} \quad R=\frac{|\beta'_\alpha|A}{2Mb}\left(\frac{1-\nu}{1+\nu}\right), \tag{26}$$

and obtain the zero energy equation for the critical thickness:

$$|\varepsilon|h^*-S\ln(4h^*)+R\left(\frac{1-e^{-kh^*}}{k}\right)=0. \tag{27}$$

In the limit where the modulation wavelength is very small, $k\to\infty$, the last term vanishes and we recover the equation for the critical thickness of a homogeneous overlayer. The opposite limit of very large modulation wavelength, $k\to 0$, gives the equation

$$(|\varepsilon|+R)h^*-S\ln(4h^*)=0, \tag{28}$$

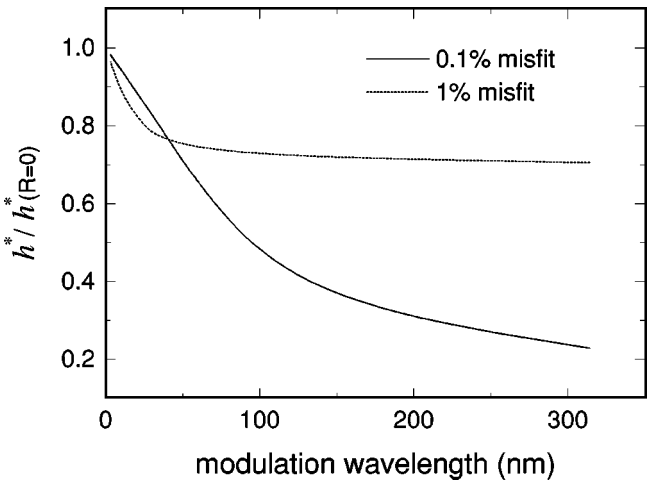

FIG. 8. The graph shows the ratio of the critical thickness for the introduction of misfit dislocations for a compositionally modulated film to the critical thickness for a homogeneous film, as a function of the wavelength of the composition modulation. The material parameters are $\nu=0.25$ and $b=0.5$ nm.

corresponding to a homogeneous overlayer of effective misfit whose absolute value is $|\varepsilon|+R$. This is because, in this limit of small k, the system looks like a single component film of the alloy element with the smallest lattice constant, effectively making the misfit more negative. If the above analysis is repeated for a film under compression, the right-hand side of Eq. (22) changes sign (since the Burgers' vector of the dislocations changes sign) and the equilibrium location of the dislocation is in the center of a stripe with the largest lattice constant. In the limit $k\to 0$, this makes the effective misfit larger. Hence, because the dislocation positions itself to effectively increase the misfit, we can say that the physical mechanism for the preferred location of the dislocation is the additional reduction in the strain energy of the overlayer.

The parameter R depends on the amplitude of the composition modulation A and the misfit between the overlayer components $\eta=-\alpha/3K$; an estimate for real systems gives $R\approx 0.1A\eta$, which is at least a factor of 10 smaller than S. Figure 8 shows the ratio of the critical thickness when $R=0.003$ to the critical thickness when $R=0$ as a function of the wavelength of the composition modulation. The value of S is 0.03 corresponding to a Poisson ratio of 1/4 and the Burger's vector has length 0.5 nm. We show the curves for values of the substrate/film misfit of 1% and 0.1%. As can be seen in the figure, a significant decrease of the critical thickness occurs as the wavelength of the composition modulation increases; this decrease is more pronounced for the 0.1% misfit since the critical thickness in the absence of the composition modulation ($R=0$) is much larger compared to the 1% misfit.

The calculation above considered the effects of the composition modulation on the behavior of the dislocations, given the initial form of the composition modulation. In a similar way, we now discuss the effects of a given distribution of misfit dislocations on the compositional ordering. This idea of using the dislocation stress field to order structures has been exploited to grow microwires in electronic devices[17] (the process involves the introduction of metallic

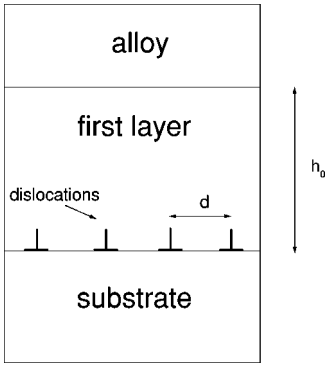

FIG. 9. Sketch of the film grown by the process discussed in the text. The first deposited layer is mismatched to the substrate and is grown until the critical thickness for the formation of an array of misfit dislocations is reached. The alloy layer is then grown by simultaneous deposition of the alloy constituents.

impurities at the surface of a thin film as it is growing; the impurities aggregate along the misfit dislocations and form the wires), and to align islands on top of growing layers.[18] The process we have in mind is the following (see Fig. 9): deposit a mismatched single-component film on a substrate until the critical thickness is reached (for example Si on Ge) and then deposit simultaneously the two-components of a compound (GaAs for example). We assume that the average lattice constant and the elastic moduli of the compound are perfectly matched to the first deposited layer and that the diffusion of atoms occurs at the surface only. The (dimensionless) distance between the growing surface and the array of edge dislocations is $h=h_0+v\tau$, with v the dimensionless speed at which the film is growing and the constant h_0 representing the critical thickness for the first deposited layer. The results from the calculations above for an array of edge dislocations in a bulk material cannot be carried over directly because of the free surface of the thin film. However, as shown in the Appendix, proper consideration of the boundary conditions at the free surface leads to the approximate dimensionless free-energy functional for the binary alloy at the surface

$$\mathcal{F}\{\psi\}=\int d\mathbf{x}\left[-\frac{\phi^2}{2}+\frac{\phi^4}{4}+\frac{|\nabla\phi|^2}{2}+\gamma\phi\frac{1}{d}\exp\left(-\frac{2\pi}{d}h\right)\cos\left(\frac{2\pi}{d}x\right)\right]. \tag{29}$$

The dynamical equation is then

$$\frac{\partial\phi}{\partial\tau}=\nabla^2\left[-\phi+\phi^3-\nabla^2\phi+\gamma\exp\left(-\frac{2\pi}{d}v\tau\right)\cos\left(\frac{2\pi}{d}x\right)\right]-v\phi, \tag{30}$$

where $\gamma=\gamma'/d\exp(-2\pi h_0/d)$. The last term in this equation accounts for the constant deposition of material that tends to mix the surface layer.

For $\gamma=0$,[13] a linear stability analysis of Eq. (30) shows that the homogeneous alloy is unstable if $v<1/4$; the competition between the decomposition and the constant deposition of material leads to the formation of lamellar patterns.

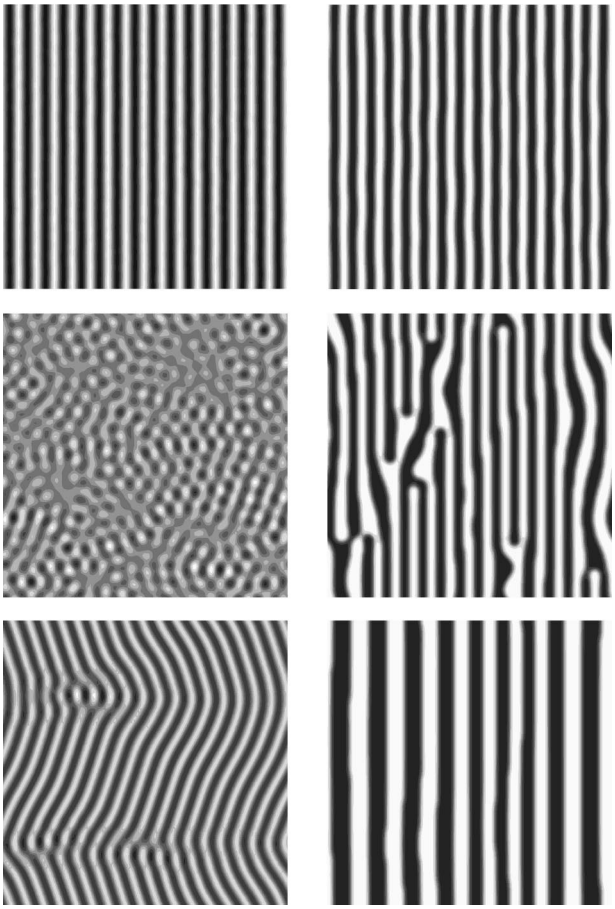

FIG. 10. Time evolution of the order parameter at the surface of a growing film in the weak segregation regime (left column) and in the strong segregation regime (right column). The spacing between the misfit dislocations is $d=10$. For the left column, the growth velocity is $v=0.24$ and the times from top to bottom are $\tau=100$, 500, and 10 000. The right panels correspond to a growth velocity $v=0.01$ and times $\tau=100$, 1000, and 10 000 from top to bottom.

For values of v close to 1/4, the pattern amplitude is small (weak segregation regime) while far below 1/4 the amplitude of the order parameter modulation is at its maximum (strong segregation regime). As time increases the value of the term due to the dislocations decreases on account of the exponential factor $\exp(-2\pi v\tau/d)$, implying that the long time behavior of the system is the same as when $\gamma=0$. At very early times, we take $\exp(-2\pi v\tau/d)\approx 1$ and solve the linear dynamical equation to obtain the time dependence of the order parameter (with the expansion $\phi=\Sigma_q\phi_q\cos qx$) as $\phi_q(\tau)=\phi_q(0)(1+\Omega\tau)+\gamma q^2\tau\delta_{q,2\pi/d}$ with $\Omega=q^2-q^4-v$. The mode $q=2\pi/d$ grows the fastest because of the term $\gamma q^2 t$ that is always present, even when $\phi_q(0)$ is made vanishingly small. The mode corresponding to the spacing of the dislocations will therefore always dominate at early times, even when the dispersion relation $\Omega(q=2\pi/d)$ is negative.

We have simulated the above dynamical equation as in the previous sections. The surface is represented by a two-dimensional square plane with periodic boundary conditions and the constant $\gamma=0.02$ in all of the simulations corresponding to order of magnitude estimates with $h_0=500$ Å, $d=200$ Å and $T_c=1000$ K. Figure 10 shows

snapshots of the surface layer at different times of the numerical simulations in the weak and strong segregation regimes. For the weak segregation regime ($v=0.24$), the initial modulation due to the dislocation array persists until a time $\tau\approx 300$, after which the long-time behavior takes over. The decay of the initial modulation proceeds by a decrease of its amplitude [due to the factor $\exp(-2\pi v\tau/d)$] until it is comparable to the amplitude of the other modes. The initial modulation will persist on a time scale that depends on the strength of the initial fluctuations in ϕ (the strength of the beam fluctuations in a real experiment), the value of γ, which determines the amplitude of the initial modulation, and on the value of $2\pi v/d$, which is responsible for the decay of the initial modulated state. The behavior of the system in the strong segregation regime is quite different, as shown in the right panels of Fig. 10. The system quickly orders in the lamellar pattern with modulation $q=2\pi/d$ due to the dislocations. As opposed to the weak segregation regime, the amplitude of the modulation stays constant throughout the dynamical evolution. At a time $\tau\approx 500$, the crossover to the long-time steady state begins: the lamellae become unstable to fluctuations, breakup, and join with neighboring stripes. This mechanism has the effect of increasing the wavelength of the modulation towards the steady-state value.

Experiments related to the deposition process described above have been reported.[19] In these experiments, a layer of GaAs was deposited on a Si substrate prior to the deposition of InGaAs. Both spinodal decomposition of the InGaAs and misfit dislocations at the GaAs/Si interface were observed, while the InGaAs/GaAs interface remained coherent. It was found that the spinodal decomposition occurred along the [110] direction, in contrast to experiments where the decomposing alloy is deposited directly on the substrate and where the decomposition occurs along the [100] and [010] directions. The difference between these experimental results could be due to the presence of the array of misfit dislocations at the GaAs/Si interface that influences the decomposition.

V. CONCLUSION

We have considered the role played by dislocations in alloys undergoing spinodal decomposition. Effective continuous free-energy functionals were derived for bulk materials containing straight, immobile dislocations and for thin films with misfit dislocations. By assuming that mechanical equilibrium is instantaneously satisfied, we showed that the displacement vector can be calculated in terms of the properties of the dislocations and as a function of the order parameter. We demonstrated that the composition dependence of the lattice constant and of the elastic moduli can induce an interaction between the composition and the stress field of the dislocations, and we calculated explicitly the form of these interactions for pure edge and screw dislocations.

For bulk systems, we presented results of numerical integrations of the dynamical equations describing the evolution of the system after a quench from a high temperature to a temperature inside the coexistence region of the phase diagram. These results showed the segregation of the two components in the stress field of the dislocations: the smaller (larger) atoms segregate to regions of compressive (tensile) stress above and below edge dislocations, the atoms with the smallest bulk and shear moduli segregate around edge dislocations, and the species with the smallest shear modulus wrap screw dislocations. The presence of an array of edge dislocations favors strongly the phase separation of the alloy components by introducing a location of choice for the interface between the components. For a random distribution of dislocations, the spinodal decomposition accelerates as the density of dislocations increases since the atoms can easily diffuse in the stress field of the dislocations to phase separate.

The equilibrium location of strain-relieving edge dislocations at the interface between a homogeneous substrate and a compositionally patterned overlayer was shown to be in the center of a stripe of the alloy element with the smallest (largest) lattice constant for films under tensile (compressive) strain, while edge dislocations that extend from the substrate to the growth surface run at the interface between two stripes. It was demonstrated that the critical thickness for the introduction of misfit dislocations in a compositionally modulated overlayer can be drastically reduced as compared to the homogeneous overlayer, and the reduction increases with the increase of the composition modulation wavelength.

We also described a crystal growth process, where a first layer is deposited on a mismatched substrate until its thickness exceeds the critical thickness for the introduction of misfit dislocations. The constituents of an alloy are then simultaneously deposited on the layer containing the misfit dislocations. The stress field of the misfit dislocations was found to decay exponentially with the critical thickness of the first layer and with the thickness of the alloy layer. To a first approximation, the stress field is periodic with a wavelength corresponding to the spacing between the misfit dislocations. At early times of the deposition process, a perfectly ordered composition pattern arises due to the misfit dislocations. For values of the dimensionless deposition rate $v>1/4$, the amplitude of the modulation decays to zero and the layer is then homogeneously mixed. For $v<1/4$, two regimes exist: when v is close to 1/4, the initial composition modulation decays in amplitude until it becomes comparable to the other modes; for v far from 1/4, the initial modulation decays by the breaking and merging of stripes. Hence, the most interesting practical situation for growing patterned films is the case where the growth velocity is large enough to preclude the phase separation.

ACKNOWLEDGMENTS

This work was supported by the NSERC of Canada. F.L. also acknowledges support from the Walter C. Sumner Fund. R.C.D. would like to thank Professor Harry Swinney and the Center for Nonlinear Dynamics at the University of Texas, Austin for hospitality during his research leave.

APPENDIX A: DERIVATION OF THE EFFECTIVE FREE ENERGY FUNCTIONAL FOR A GROWING THIN FILM

We assume that the system is semi-infinite in the y direction with a free surface at $y=h$ and an array of edge dislo-

cations of spacing d with Burgers vector $\mathbf{b}=b\hat{\mathbf{x}}$. The boundary conditions require that the stresses vanish as $y\rightarrow-\infty$ and that $\sigma_{xy}=\sigma_{yy}=\sigma_{zy}=0$ at the free surface. We are interested in lateral phase separation at the free surface, and therefore take the order parameter gradient in the y direction to vanish. This ensures that the contributions to σ_{zy} and σ_{xy} from spatial variations in the order parameter are equal to zero. The order parameter contribution to σ_{yy} also vanishes due to the mechanical equilibrium condition. Since the z axis is parallel to the dislocation lines, the displacement vector is independent of z and $u_z=0$, implying that $\sigma_{zy}=0$. The procedure to cancel σ_{xy} and σ_{yy} at the free surface is as follows:[20] first introduce an image dislocation at $y=2h$ (this cancels σ_{xy}) and then add a stress function that will eliminate the resulting σ_{yy}. The value of σ_{yy} to be eliminated after the image dislocation is introduced is

$$\sigma_{yy}=\frac{2M}{1+\nu}\left(\frac{b}{2\pi}\right)\left[-\frac{2\nu}{1-\nu}\sum_{n=-\infty}^{\infty}\frac{h}{(x-nd)^2+h^2}+\sum_{n=-\infty}^{\infty}\frac{(x-nd)^2h-h^3}{[(x-nd)^2+h^2]^2}\right]. \tag{A1}$$

The terms in this expression are written in such a way that the summation is well behaved. Evaluation of these sums gives the expressions

$$\sum_{n=-\infty}^{\infty}\frac{h}{(x-nd)^2+h^2}=\frac{\pi}{2d}\frac{\sinh 2\phi}{\cosh^2\phi-\cos^2\theta} \tag{A2}$$

and

$$\sum_{n=-\infty}^{\infty}\frac{(x-nd)^2h-h^3}{[(x-nd)^2+h^2]^2}=\frac{h\pi^2}{d^2}\frac{\cos^2\theta\cosh^2\phi-\sin^2\theta\sinh^2\phi}{[\cos^2\theta\cosh^2\phi+\sin^2\theta\sinh^2\phi]^2}. \tag{A3}$$

The angular variables ϕ and θ are defined as $\phi=(h/d)\pi$ and $\theta=(x/d)\pi$. The hyperbolic functions can be approximated by $\sinh\phi\approx\cosh\phi\approx 1/2\exp(\phi)$ when ϕ is not too small, giving the ratio of the second sum to the first sum proportional to $(h/d)\exp(-2\phi)$. Hence, the second term in Eq. (A1) can be neglected.

We now introduce the stress function Ψ that satisfies the mechanical equilibrium equation $\nabla^4\psi=0$ and from which the stresses can be calculated as $\sigma_{yy}=\partial^2_{yy}\Psi$ and $\sigma_{xy}=-\partial^2_{yx}\Psi$. Separation of variables with the boundary conditions $\Psi\rightarrow 0$ as $y\rightarrow-\infty$ and that the addition of ψ does not produce a shear stress σ_{xy} at the surface, gives the solution

$$\Psi=2M\frac{2\nu}{(1+\nu)(1-\nu)}\frac{b}{2\pi^2}[(y-h)I_1-I_2], \tag{A4}$$

where I_1 and I_2 are given by

$$I_n=\int_0^{\infty}k^{-n}e^{k(y-h)}I(k)\cos(kx)dk. \tag{A5}$$

In this last expression, $I(k)$ is given by

$$I(k)=\int_{-\infty}^{\infty}\left(\sum_{n=-\infty}^{\infty}\frac{h}{(x-nd)^2+h^2}\right)\cos(kx)dx. \tag{A6}$$

The expression for Ψ can then be used to compute the elastic free energy at the surface from Eq. (2):

$$\mathcal{F}_{el}\{\psi\}=\int d\mathbf{r}\left[(\alpha'\psi+\beta'\nabla_x^2\nabla^{-2}\psi)\sum_{n=-\infty}^{\infty}\frac{h}{(x-nd)^2+h^2}\right]. \tag{A7}$$

The new coefficients α' and β' are given by

$$\alpha'=\alpha\frac{8M-3K}{3M}\frac{2\nu(1-2\nu)}{(1-\nu)^2}\frac{b}{2\pi} \tag{A8}$$

and

$$\beta'=-\alpha\frac{6M\beta}{3K+4M}\frac{1-\nu-2\nu^2}{(1-\nu)^2}\frac{b}{2\pi}. \tag{A9}$$

Neglecting terms as discussed above, the dimensionless elastic functional integral can be written as

$$\mathcal{F}_{el}\{\phi\}=\int d\mathbf{x}\left[\gamma'\phi\frac{1}{d}\exp\left(-\frac{2\pi}{d}h\right)\cos\left(\frac{2\pi}{d}x\right)\right], \tag{A10}$$

with the constant $\gamma'=(\alpha'+\beta')r^{-1}(u/c)^{1/2}$.

[1] A. H. Cottrell, *Dislocations and Plastic Flow in Crystals* (Oxford University Press, London, 1953).

[2] C. C. Dollins, Acta Metall. **18**, 1209 (1970).

[3] J. W. Cahn, Acta Metall. **5**, 169 (1957); G. Sundar and J. J. Hoyt, J. Phys. Condens. Matter **4**, 4359 (1992).

[4] For a review, see F. C. Larché, in *Dislocations in Solids*, edited by F. R. N. Nabarro (North-Holland, New York, 1979), Vol. 4.

[5] J. W. Cahn, Acta Metall. **11**, 1275 (1963).

[6] A. Sato, K. Tamura, M. Ito, M. Kato, and T. Mori, Acta Metall. Mater. **41**, 1047 (1993).

[7] R. R. Bhat and P. P. Rao, Z. Metallkd. **75**, 237 (1994).

[8] S. Spooner and B. G. Lefevre, Metall. Trans. A **11A**, 1085 (1980).

[9] J. T. Plewes, Metall. Trans. A **6A**, 537 (1975).

[10] F. K. Legoues, MRS Bull. **21**, 38 (1997).

[11] W. A. Jesser and J. H. van der Merwe, in *Dislocations in Solids*, edited by F. R. N. Nabarro (North-Holland, New York, 1989), Vol. 8; C. A. B. Ball and J. H. van der Merwe, *ibid.* (1983), Vol. 6; J. H. van der Merwe, J. Appl. Phys. **34**, 117 (1963); **34**, 123 (1963); F. C. Frank and J. H. van der Merew, Proc. R. Soc.

London, Ser. A **200**, 125 (1949).
[12] J. W. Matthews and A. E. Blakeslee, J. Cryst. Growth **32**, 265 (1976); **29**, 273 (1975).
[13] F. Léonard and R. C. Desai, Phys. Rev. B **56**, 4955 (1997); **57**, 4805 (1998).
[14] L. D. Landau and E. M. Lifshitz, *Theory of Elasticity* (Addison-Wesley, Reading, MA, 1986).
[15] J. D. Eshelby, in *Progress in Solid Mechanics*, edited by I. N. Sneddon and R. Hill (North-Holland, Amsterdam, 1961), Vol. 2, p. 89.
[16] J. W. Cahn and J. E. Hilliard, J. Chem. Phys. **28**, 258 (1958).
[17] D. M. Lee, J. B. Posthill, and G. A. Rozgonyi, in *Dislocations and Interfaces in Semiconductors* (Metallurgical Society, Warrendale, PA., 1988); A. S. M. Salih, H. J. Kim, R. F. Davis, and G. A. Rozgonyi, Appl. Phys. Lett. **46**, 419 (1985).
[18] D. E. Jesson, K. M. Chen, S. J. Pennycook, T. Thundat, and R. J. Warnack, Science **268**, 1161 (1995).
[19] A. Georgalikas, A. Dimoulas, A. Christou, and J. Stoemenos, J. Mater. Res. **7**, 2194 (1992).
[20] J. P. Hirth and J. Lothe, *Theory of Dislocations* (McGraw-Hill, New York, 1968).